Atmos. Chem. Phys. Discuss., 12, 30081–30117, 2012
www.atmos-chem-phys-discuss.net/12/30081/2012/
doi:10.5194/acpd-12-30081-2012

Atmospheric Chemistry and Physics Discussions

Transport of aerosol pollution in the UTLS during Asian summer monsoon as simulated by ECHAM5-HAMMOZ model

S. Fadnavis[1], K. Semeniuk[2], L. Pozzoli[3], M. G. Schultz[4], S. D. Ghude[1], and S. Das[1]

[1]Indian Institute of Tropical Meteorology, Pune, India
[2]Center for Research in Department of Earth and Space Sciences, York University, Toronto, Canada
[3]Eurasia Institute of Earth Sciences, Istanbul Technical University, Turkey
[4]Institute for Energy and Climate Research-Troposphere (IEK-8), Forschungszentrum, Julich, Julich, Germany

Received: 17 October 2012 – Accepted: 7 November 2012 – Published: 21 November 2012

Correspondence to: S. Fadnavis (suvarna@tropmet.res.in) and
K. Semeniuk (kirill@cumulus.eas.yorku.ca)

Published by Copernicus Publications on behalf of the European Geosciences Union.

Abstract

An eight member ensemble of ECHAM5-HAMMOZ simulations for the year 2003 is analyzed to study the transport of aerosols in the Upper Troposphere and Lower Stratosphere (UTLS) during the Asian Summer Monsoon (ASM). Simulations show persistent maxima in black carbon, organic carbon, sulfate, and mineral dust aerosols within the anticyclone in the UTLS throughout the ASM (period from July to September) when convective activity over the Indian subcontinent is highest. Model simulations indicate boundary layer aerosol pollution as the source of this UTLS aerosol layer and identify ASM convection as the dominant transport process. Evidence of ASM transport of aerosols into the stratosphere is observed in HALogen Occultation Experiment (HALOE) and Stratospheric Aerosol and Gas Experiment (SAGE) II aerosol extinction. The impact of aerosols in the UTLS region is analyzed by evaluating the differences between simulations with (CTRL) and without aerosol (HAM-off) loading. The transport of anthropogenic aerosols in the UTLS increases cloud ice, water vapour and temperature, indicating that aerosols play an important role in enhancement of cloud ice in the Upper-Troposphere (UT). Aerosol induced circulation changes include a weakening of the main branch of the Hadley circulation and increased vertical transport around the southern flank of the Himalayas and reduction in monsoon precipitation over the India region.

1 Introduction

East Asia is one of the largest gaseous and aerosol pollutant source regions, having both high anthropogenic emissions and important natural sources such as wildfires and dust storms (Park et al., 2010; Jeong et al., 2011). Developing nations of East Asia are experiencing dramatic levels of aerosol pollution, because of the rapid push to industrialization (Liu and Diamond, 2005; Venkataraman et al., 2005). The increase in atmospheric concentrations of man-made aerosols (including black carbon, organic

ACPD
12, 30081–30117, 2012

carbon, and sulfate) from such sources as transportation, industry, agriculture, and urban land development affect weather and climate (IPCC, 2007). Absorbing aerosols such as dust and black carbon heat the atmosphere due to shortwave absorption. Non-absorbing aerosols such as sulfate cause surface cooling by scattering solar radiation, but have a relatively small heating effect on the atmosphere itself. Both absorbing and non-absorbing aerosols cause a solar dimming effect by blocking part of the solar radiation from reaching the earth surface (Ramanathan et al., 2005; Lau et al., 2006). Recent studies suggest that increased aerosol loading may change the energy balance in the atmosphere and at the Earth's surface, and alter the global water cycle (IPCC, 2007). Ramanathan et al. (2005) reported that the polluted layer of black carbon, organic carbon and dust over the Asian monsoon region leads to a weakening of the summer monsoon rainfall. However, Lau et al. (2006) argued that absorbing aerosols over the elevated Tibetan Plateau with its high surface albedo intensify the Indian summer monsoon through the increased heat pump effect. Numerical experiments have suggested that atmospheric circulation anomalies induced by black carbon may be a cause of drought over Northern China and of excessive rain fall over Southern China and India (Menon et al., 2002). These studies indicate that aerosol effects can induce large changes in precipitation patterns, which in turn may change the Earth's climate.

Recent satellite observations reveal that the ASM circulation provides a pathway for pollution transport into the stratosphere (Randel et al., 2010) and thus causes a large and discernible chemical influence on the stratosphere. A persistent maximum of tropospheric chemical constituents (H_2O, CO, C_2H_6, CH_4, N_2O, HCN, and aerosols) are observed inside the ASM anticyclone in the UTLS during boreal summer (Park et al., 2004; Li et al., 2005; Randel and Park, 2006; Fu et al., 2006; Xiong et al., 2009; Randel et al., 2010). The anticyclonic circulation and constituent maxima extend into the lower stratosphere (Park et al., 2007). Satellite observations and model simulations have shown rapid transport of boundary level pollution from Asia, India and Indonesia into the anti-cyclonic circulation is associated with the ASM. Recently, transport of aerosols to the upper troposphere by deep convection over the Asian monsoon regions has been

ACPD
12, 30081–30117, 2012

observed in CALIPSO lidar measurements (Vernier et al., 2011). This aerosol layer extends from Eastern Mediterranean to Western China and vertically from 13 to 18 km. Observations and modeling studies suggest that the occurrence of aerosol layers near the tropopause that have been advected through long-range transport could strongly affect cloud microphysical processes and precipitation formation (Li et al., 2005; Yin et al., 2005; Su et al., 2011). The influence of anthropogenic aerosol (sulfate and soot) on upper tropospheric (UT) clouds through ice nucleation was studied by Liu et al. (2009) using the NCAR Community Atmospheric Model Version 3 (CAM3). They reported that the homogeneous freezing of sulfate particles dominates cirrus cloud formation in the upper troposphere. The anthropogenic sulfate results in a global annual mean change of long-wave cloud forcing (LWCF) of $0.20 \pm 0.09\,\mathrm{W\,m^{-2}}$ and short-wave cloud forcing (SWCF) of $0.30 \pm 0.17\,\mathrm{W\,m^{-2}}$ and an increase of UTLS water vapor by $\sim 10\,\%$. When both homogeneous and heterogeneous ice nucleation and their competition are allowed, anthropogenic soot may increase global cirrus cloud cover by $\sim 2\,\%$ and UTLS water vapor by 40 % with a change in LWCF of $1.5\,\mathrm{W\,m^{-2}}$. Recently, it became clear that cirrus clouds significantly affect the global energy balance and climate, due to their influence on atmospheric thermal structure. From satellite observations Su et al. (2011) hypothesized that aerosol semi-direct radiative heating and change in cirrus radiative heating may contribute to the observed increase in tropical tropopause layer temperatures and to elevated water vapour concentrations in polluted clouds. Several other studies (e.g. Randall et al., 1989; Ramaswamy and Ramanathan, 1989; Liu et al., 2003a,b) pointed out that cirrus clouds are likely to have a great impact on the radiation and hence affect the intensity of the large-scale circulation in the tropics (Dodion et al., 2008).

Aerosols have much longer residence time in the stratosphere than in the troposphere and they get dispersed over a larger area. Through their interaction with ultraviolet, visible and infrared radiation, stratospheric aerosols are likely to play a significant role in the Earth's radiation budget and climate (Dodion et al., 2008). Continuous emission of sulfur into the tropical lower stratosphere could lead to heating of

ACPD
12, 30081–30117, 2012

the tropical tropopause layer (Heckendorn et al., 2009). Simulations of stratospheric geo-engineering with black carbon (BC) aerosols using a general circulation model with fixed sea surface temperatures show that 1 Tg BC per year injected into the lower stratosphere would cause stratospheric warming of over 60 °C (Kravitz et al., 2012).

In this study we simulate and analyze the transport of aerosols from the polluted surface of South East Asia to the anticyclone over the Tibetan Plateau. Further we investigate the potential impact of aerosols on the UTLS region. We employ the state of the art ECHAM5-HAMMOZ aerosol-chemistry-climate model (Pozzoli et al., 2008a, 2011) to simulate black carbon (BC), organic carbon (OC), mineral dust and sulfate (SO_4^{2-}) aerosols during boreal summer 2003. The model results are evaluated through a comparison with HALOE and SAGE II data. To understand the effect of aerosols on the UTLS region the difference between model simulations with aerosols loading (CTRL) and without aerosols loading (HAM-off) are analyzed. The paper is organized as follows. The ECHAM5-HAMMOZ model and satellite data (SAGE II and HALOE) are described in Sect. 2. The influence of ASM convection on the distribution of aerosols in the UTLS is discussed in Sect. 3.1 and impact of aerosols on cloud ice, temperature, water vapor and changes in circulation and precipitation are presented in Sect. 3.2. Section 4 concludes this study.

2 Model simulations and data analysis

2.1 ECHAM5-HAMMOZ model simulation and experimental setup

The ECHAM5-HAMMOZ aerosol-chemistry-climate model used in the present study comprises the general circulation model ECHAM5 (Roeckner et al., 2003), the tropospheric chemistry module, MOZ (Horowitz et al., 2003), and the aerosol module, Hamburg Aerosol Model (HAM) (Stier et al., 2005). The tropospheric chemistry module MOZ and the aerosol module HAM are fully interactive and implemented together in ECHAM5 (Pozzoli et al., 2008a). The HAM module takes into account the major

ACPD
12, 30081–30117, 2012

aerosol compounds namely sulfate, black carbon, organic carbon, sea salt and mineral dust. It represents aerosols as internal and external mixtures with four soluble and three insoluble modes (Vignati et al., 2004). Details of the aerosol categorization and their parameterization schemes are documented by Stier et al. (2005). The chemical scheme used in the tropospheric chemistry module, MOZ is identical to MOZART-2 model with small modifications as described by Pozzoli et al. (2008a). It includes 63 tracers and 168 reactions to represent O_x-NO_x-hydrocarbon chemistry.

We used the RETRO project data set of the year 2000 (http://www.retro.enes.org/) for the surface CO, NO_x, and hydrocarbon emissions from anthropogenic sources and biomass burning emissions (Schultz et al., 2008). The anthropogenic and fire aerosol emissions are based on the AEROCOM emission inventory (Dentener et al., 2006) representative of the year 2000. The emissions are described in detail by Pozzoli et al. (2008a,b). Stratospheric NO_x, HNO_3, and CO concentrations are supplied as 3-D monthly means from simulations of the MOZART-3 model (Kinnison et al., 2007). Stratospheric O_3 concentrations are prescribed as monthly mean zonal climatology derived from observations (Randel et al., 1998; Logan, 1999). These concentrations are fixed at the topmost two model levels (pressures of 30 hPa and above). At other model levels above the tropopause, the concentrations are relaxed toward these values with a relaxation time of 10 days following Horowitz et al. (2003). The tropopause height is diagnosed as the lowest level at which the lapse rate decreases to $2\,^{\circ}\mathrm{C\,km^{-1}}$ or less following the World Meteorological Organization definition (WMO, 1992).

The ECHAM5, HAM and MOZ model performance against observations have been presented in earlier studies (e.g. Stier et al., 2005; Auvray et al., 2007; Pozzoli et atl., 2008a,b; Rast et al., 2012). Evaluation of the simulated distributions of trace gas and aerosol over the Pacific during the TRACE-P aircraft experiment has been reported by Pozzoli et al. (2008a). Stier et al. (2005) found good agreement between simulated and observed sulfate, black carbon and organic carbon surface concentrations regionally. In general good agreement was found between simulated variables and observations.

ACPD
12, 30081–30117, 2012

Simulations were performed using the coupled model ECHAM5-HAMMOZ with a spectral resolution of T42 corresponding to about $2.8 \times 2.8^{\circ}$ in the horizontal dimension and 31 vertical hybrid σ-p levels from the surface up to 10 hPa. Time step length was 20 min. To study the influence of ASM deep convection on the distribution of aerosols, we carry out 8-member ensemble runs for the ASM season (June–September) starting from initial conditions of 24–31 March for each year 2000–2004. The climatology of AMIP2 SSTs representative of the period 1995–2004 was specified as a lower boundary condition.

During boreal summer in 2003, the equatorial quasi-biennial oscillation (QBO) was in a weak easterly phase in the lower stratosphere (Randel and Park, 2006; Bowman, 2006). Such periods are associated with transport induced by Rossby wave breaking (e.g. O'Sullivan and Dunkerton, 1997; Haynes and Shuckburgh, 2000). Hence, the equatorial UTLS is less isolated from intrusions of subtropical and extra-tropical air masses. In particular, the polluted air injected via the ASM anticyclone may be transported to the equator and into the Southern Hemisphere. Although similar features are observed during 2000–2004, monsoon circulation effects on distribution of aerosols are well marked during the year 2003. Hence, in the present study analysis is presented for the year 2003. The simulations were conducted for (1) the base line simulations with aerosol mixing ratios calculated on-line (CTRL) and (2) simulations without aerosol mixing ratios on-line calculations (HAM-off). In the CTRL simulation the simulated aerosol concentrations are used in the calculation of the radiative budget and of the cloud droplet (CDNC) and the ice crystal (ICNC) concentrations according to Stier et al. (2005), Lohmann et al. (1999), Lin and Leaitch (1997), respectively. The HAM-off simulation includes the standard ECHAM5 cloud scheme (Lohmann and Roeckner, 1996; Roeckner et al., 2003), without interactions between aerosols, radiative budget, cloud droplet and ice crystal concentrations. We analyze the difference between these two simulations CTRL – HAM-off to quantify the influence of aerosols on temperature, water vapour, cloud ice, circulation and precipitation.

ACPD
12, 30081–30117, 2012

2.2 Satellite observations: SAGE II and HALOE

Here we present analyses of the distribution of aerosol extinction from two satellite based instruments namely Stratospheric Aerosol and Gas Experiment II (SAGE II) aboard the Earth Radiation Budget Satellite (ERBS) and Halogen Occultation Experiment (HALOE) aboard the Upper Atmospheric Research Satellite (UARS). HALOE is a limb-viewing solar occultation instrument that obtains transmittance profiles in the infra-red region of the spectrum giving 15 sunrise and 15 sunset measurements each day (Russell et al., 1993). HALOE was operational from September 1991 to November 2005. The vertical resolution is ∼2 km or less. Temporal and spatial coverage of HALOE are similar to those of SAGE II (Terao and Logan, 2007). Measurements in eight infrared bands (2.45–10.01 µm) are used to retrieve the profiles of seven trace gas mixing ratios (HCl, CH_4, HF, NO, NO_2, O_3, H_2O). Temperature and aerosols are retrieved at four wavelengths (2.45, 3.40, 3.46, 5.26 µm). The HALOE aerosol retrievals are described in detail by Hervig et al. (1995). The validation of these measurements suggests uncertainties of ∼15–20 % (Hervig et al., 1995). Aerosol extinction at 5.26 µm is analyzed to study transport of aerosols in the UTLS region. HALOE data are available at: http://haloe.gats-inc.com/download/index.php.

The SAGE II data used here are based on the v6.2 retrieval algorithm. SAGE II is also a solar occultation instrument where measurements are only made during limb viewing conditions providing 15 sunrise and 15 sunset measurements per day. During each sunrise and sunset encountered by the orbiting spacecraft, the instrument uses the solar occultation technique measuring the attenuated solar radiation through the Earth's limb in seven channels with central wavelengths ranging from 0.385 µm to 0.1020 µm. The transmittance measurements are inverted using the "onion-peeling" approach (Antuña et al., 2002) to retrieve the aerosol extinction coefficient (km^{-1}) as well as the other atmospheric compounds such as ozone, nitrogen dioxide, and water vapor at 0.385 µm, 0.453 µm, 0.525 µm, and 0.1020 µm. SAGE II has a horizontal resolution of the order of 200 km and a vertical resolution of 1 km (Kent et al., 1998).

ACPD
12, 30081–30117, 2012

SAGE II aerosol data has been validated by Oberbeck et al. (1989) indicating an extinction uncertainty of ∼20–30 %. To keep uniformity with HALOE aerosol extinction 5.26 µm, SAGE II aerosol extinction data (km^{-1}) at 0.525 µm are analyzed. SAGE II data is available from: ftp://ftp-rab.larc.nasa.gov/pub/sage2/v6.20.

3 Results and discussions

3.1 Transport of aerosols in the UTLS region due to ASM

In order to study the influence of ASM convection on the distribution of aerosols in the UTLS monthly mean concentrations of black carbon (BC), sulfate (SO_4^{2-}), organic carbon (OC) and mineral dust aerosols from the ECHAM5-HAMMOZ ensemble are analyzed for the year 2003. These monthly mean aerosols concentration ($ng\,m^{-3}$) are then averaged during ASM (June–September) to show seasonal variation. Figure 1 shows the distributions of BC, SO_4^{2-}, OC, and mineral dust aerosol, respectively at 110 hPa averaged during ASM 2003. Similar distribution is observed during every month of ASM. Figure 1a also displays the average wind field at the same pressure level. The winds show a strong anticyclonic circulation between 20°–120° E, 12°–40° N collocated with a maximum in all aerosol fields. Confinement of aerosols within the anticyclonic circulation, with a pronounced maximum on its eastern part covering South-East Asia and India is quite obvious in Fig. 1a–d.

An aerosol maximum near the tropopause is the fingerprint of AMS influence. CALIPSO lidar measurements have revealed the existence of an aerosol layer at the tropopause associated with the Asian monsoon season and its confinement in the anticyclonic circulation with vertical extent from 13–18 km (Vernier et al., 2011). Global Ozone Monitoring by Occultation of Stars (GOMOS) and Advanced Composition Explorer (ACE) aerosol annual extinctions during 2004–2005 also show an aerosol maximum in the tropics at an altitude of 15–17 km (Dodion et al., 2008). Also, a number of studies have reported a persistent maximum of other tropospheric chemical

ACPD
12, 30081–30117, 2012

constituents (H_2O, CO, CH_4, N_2O, HCN) inside the Asian summer monsoon anticyclone in the UTLS during ASM (Gettelman et al., 2004; Li et al., 2005; Fu et al., 2006; Randel and Park, 2006; Park et al., 2007; Randel et al., 2010). Satellite observations (Park et al., 2007) and model simulation (Park et al., 2009) studies have shown rapid transport of boundary level pollution from Asia, India and Indonesia into the anticyclonic circulation.

To understand vertical transport, longitude-pressure and latitude-pressure cross-sections of distribution of aerosols in the anticyclonic region are analyzed. Figure 2 shows longitude-pressure cross-section (averaged for 15–35° N and for June–September) of aerosols as obtained from ECHAM5-HAMOZ CTRL simulations. In agreement with satellite observations ECHAM5-HAMMOZ simulations show a layer of aerosols in the UTLS region (∼ between 416 hPa and 70 hPa). Transport of boundary layer aerosols from 60–120° E to the UTLS region due to large scale monsoon convection is quite evident. There are two regions of vertical transport apparent eastward of 60° E, first at the eastern end of the anticyclone (around 85° E) and second around 120° E. This second region over the South China Sea is another pathway for aerosols into the UTLS and it is likely that some of this aerosol is transported westward by the equatorial easterly winds and is trapped in the anticyclone as identified by the aerosol maximum around 85° E and 110 hPa. The latitude-pressure cross-sections (averaged over 60° E–120° E) of aerosol fields (BC, OC, SO_4^{2-} and mineral dust) averaged during the Asian monsoon season are plotted in Fig. 3. Cross-tropopause transport (extending up to 70 hPa) is evident in all the aerosol distributions, but the details vary. Similar transport is observed during every month (June–September) for all the aerosol fields. A pronounced maximum near 30° N is associated with the ASM anticyclone. High concentrations of BC, OC, SO_4^{2-} and mineral dust in the UTLS extend to the equator and are then transported poleward and downward in the Southern Hemisphere to ∼ 30° S due to Brewer–Dobson circulation. Most of the transport appears to occur just above the tropical tropopause suggesting mixing by breaking Rossby waves in the lower tropical stratosphere. This is consistent with the fact that 2003 had weak QBO easterlies

ACPD
12, 30081–30117, 2012

during June–September in the lower tropical stratosphere, which would reduce the isolation of the tropics from Rossby wave propagation (Andrews et al., 1987). In addition, the tropical stratosphere in this layer tends to be poorly isolated from the extratropics (Minschwaner et al., 1996). Similar transport is also observed in ACE-FTS observations of HCN (Randel et al., 2010). From Figs. 2 and 3 one can also infer that large scale vertical transport within the anticyclone is related to deep monsoon convection over the region 10–35° N, 60–120° E.

Figure 4 shows emissions of black carbon, organic carbon, mineral dust and sulfur over the Asian region and surrounding area. Sulfur missions are primarily from coal-fired power plants. Asia is one of the highest sulfur producing regions in the world (Vernier et al., 2011). The industrial and residential sectors emit BC and OC which are produced through incomplete combustion of coal and bio-fuel and also in wildland fires. These emissions are high over South West China and the Indo Gangetic Plain (IGP) of India. Source regions of high mineral dust are in the North Africa, the North-West China Taklimakan desert, part of Arabia, Iran and the shores of the Caspian Sea. The low level convergence during ASM may collect these pollutants from the aforementioned regions and deep convective activity lifts them upward. As can be seen in Figs. 2 and 3, transport of aerosols in the UTLS primarily occurs over convective region (15–30° N, 60–120° E). As noted above a major route for this convective transport is over Northern India on the southern flanks of the Himalayas. There is deep convective transport over the South China Sea region as well.

Altitude-latitude cross sections of aerosol extinction obtained from HALOE (5.26 µm) and SAGE II (0.525 µm) and ECHAM5-HAMMOZ CTRL simulations (0.550 µm), averaged over longitudes 60–120 °E and for the ASM season of the year 2003 are shown in Fig. 5a–c, respectively. Since the number of profiles obtained from HALOE are less at altitudes below 16 km over the ASM region, aerosol extinction is plotted over the altitudes 16–32 km. Figure 5a, b shows evidence of enhanced aerosol concentrations in the lower stratosphere transported into the Southern Hemisphere across the equator with descent over the southern subtropics. The ECHAM5-HAMMOZ simulation

ACPD
12, 30081–30117, 2012

produced similar transport (see Fig. 5c). As the Asian summer monsoon transport of pollution occurs every year (Park et al., 2009; Kunze et al., 2010; Vernier et al., 2011), similar variation of aerosols is also observed in ACE 2005 measurements (see Fig. 6 in Dodion et al., 2008). Dodion et al. (2008) reported that the observed aerosol layer indicates the presence of high subvisible cirrus clouds. They also observed a correlation of latitudinal variation of cirrus clouds with seasonal variation of the Inter-tropical convergence zone (ITCZ), which is indicative of dependence on aerosol redistribution.

Deep convection occurs frequently over the region spanned by 15–30° N and 60–120° E. Time series of Outgoing Long-wave Radiation (OLR) averaged over this region is an indicator of convective forcing; hence it used as a proxy of monsoon convection (Randel and Park, 2006). Association of deep convection with aerosols in the UTLS is examined by observing simultaneously time variations of OLR and BC, OC and SO_4^{2-} aerosols at 110 hPa averaged over the central monsoon region (20–30° N, 60–120° E). Figure 6 illustrates the coupling of deep convection with aerosol transport within the anticyclone. A 10–20 day periodicity in convection is evident in the aerosols. Time series of BC, OC and SO_4^{2-} aerosols mixing ratio show statistically significant (at 95 % confidence level) anti-correlation greater than 0.5 with OLR, thus all the aerosols vary coherently with OLR. During the strongest deep convective event in late June aerosol concentrations abruptly increase and they remain relatively high during the monsoon season. Similar coherent variation of water vapour and convection was observed in AIRS data (Randel and Park, 2006). This indicates that the model is able to qualitatively reproduce the influence of AMS convection on UTLS aerosols.

Li et al. (2005) proposed that uplifted boundary layer aerosols trapped by the Tibetan anticyclone could enhance high altitude cloud formation and would have consequences for precipitation. From Microwave Limb Sounder (MLS) observations they showed evidence of elevated ice water content collocated with a pollution-generated CO maximum during the ASM. GOMOS and ACE-FTS measurements also showed the coexistence of an aerosol layer and sub-visual tropical cirrus clouds during 2004 and 2005 at an altitude of 15–17 km (Dodion et al., 2008). Spatial distribution of ECHAM5-HAMMOZ

ACPD
12, 30081–30117, 2012

(CTRL runs) simulated Ice Cloud Water (ICW) and Ice Crystal Number Concentration (ICNC) at 110 hPa are shown in Fig. 7a, b. It shows high amounts IWC and ICNC at the eastern flank of anticyclone. Figure 7c and d exhibit time average and latitude-pressure cross sections (averaged over 60° E–120° E) of ICW and ICNC. Maxima in ICW and ICNC collocated with the aerosol maximum (Fig. 1) indicate that transport of aerosol and water vapour rich air by ITCZ may enhance cloud ice formation in the Northern Hemisphere subtropics. High amounts of ICW and ICNC near the tropical tropopause layer indicate that uplifted boundary layer aerosols trapped by the Tibetan anticyclone may elevate cloud ice formation. The distribution of ICW and ICNC in this region is consistent with the aerosol distributions shown in Figs. 3 and 5. High amounts of ICW and ICNC at lower latitudes are related to deep convection partly over the Indian Ocean and partly over South-east Asia and the Indonesian archipelago. So the ICW and ICNC concentrations between 10°–20° N are related to the ASM and appear to be consistent with the aerosol distributions shown in Fig. 5.

In simulations using the NCAR-CAM3 model coupled to the IMPACT global model, Liu et al. (2009) reported that in HOM scenario (the homogeneous freezing of sulfate particles dominates cirrus cloud formation) anthropogenic sulfate emissions resulted in an increase of cloud ice number by 10 % and cirrus cloud cover by 3–5 %, over the tropical upper troposphere. In HET scenario (homogeneous and heterogeneous ice nucleation and their competition were allowed) ice number concentration was increased by 30 % and global cirrus cloud cover by ∼2 %. In agreement with Liu et al. (2009), high amounts ICW and ICNC in the tropical upper troposphere in the present study indicate that sulfate and soot aerosols likely have enhanced cloud ice formation.

3.2 Impact of aerosols on the UTLS region

Next we consider the impact of aerosols on the UTLS region. Processes in the UTLS have an impact on the radiative and chemical balance of the atmosphere. The difference between CTRL and HAM-off simulations (aerosol induced anomalies) is shown in Figs. 8–10. Figure 8a shows the horizontal distribution of the aerosol induced cloud

ACPD
12, 30081–30117, 2012

ice ($\mu g\,m^{-3}$) anomalies at 181 hPa averaged during the ASM season. It shows a prominent feature at the eastern end of the anticyclone region where the positive cloud ice anomaly has a maximum over 1500 $\mu g\,m^{-3}$. Based on present day and pre-industrial scenarios, Liu et al. (2009) also reported increase in aerosol induced (sulfate and black carbon) cloud ice anomalies (0–0.6 $mg\,kg^{-1}$) in the tropical upper troposphere. ECHAM5-HAMMOZ simulated cloud ice anomalies the tropical upper troposphere varies between 0.3–1.5 $mg\,kg^{-1}$, this broadly agrees with Liu et al. (2009). Figure 8b shows the time (ASM) and zonal average (60° E–120° E) latitude versus pressure cross section of aerosol induced cloud ice anomalies ($\mu g\,m^{-3}$). It can be seen that cloud ice shows increases up to 10 $\mu g\,m^{-3}$ near the tropical tropopause due to aerosol loading. There is also cloud ice increase around 20° N which connects the lower troposphere to the upper troposphere and is associated with a region of enhanced vertical transport (see Fig. 9). Increases of cloud ice near the tropical tropopause are associated with warming due to increased reflection of upwelling infrared radiation by cirrus clouds. Lau et al. (2006) and Lau and Kim (2006) reported that radiative heating of absorbing aerosols (mineral dust and BC) may cause upper tropospheric warming over the Tibetan Plateau during Asian summer monsoon season. The radiative heating from subvisible cirrus clouds near the tropopause can act to increase water vapour entering the stratosphere by increasing tropopause temperature (Rosenfield et al., 1998). However, this effect is not captured here as subvisible cirrus clouds are not parameterized in the model.

Figure 9a, b shows the aerosol induced change in the temperature and water vapour. The change in the meridional circulation is shown as well. There is an increase in temperature (∼ 1–5 K) near the tropical tropopause. A similar increase in temperature is reported by Lau et al. (2006), Lau and Kim (2006), Liu et al. (2009), Su et al. (2011). The interior of the anticyclone over the Tibetan Plateau experiences a significant warming as well but the warming is greater than that found by Lau et al. (2006).

The aerosol induced meridional circulation anomaly shows descent (or decreased ascent) at about 0–10° N and 35–40° S (Fig. 9b). This pattern indicates a slight

ACPD
12, 30081–30117, 2012

contraction and weakening of the dominant Hadley circulation cell which straddles the equator. A weakening of the Hadley circulation due to aerosol forcing is consistent with the findings of Ramanathan et al. (2005) and Bollasina et al. (2011) although there are significant differences in the model scenarios being considered. Weaker upwelling in the ITCZ around 5° N is associated with reduced water vapour transport into the middle troposphere and warmer temperatures at the cold point due to lower cloud top heights. It also produces a cooling around 7 km and 5° N from reduced release of latent heat by cloud condensate.

A weak descent anomaly at the tropical tropopause is seen in Fig. 9. This reduction in upwelling through the tropical tropopause is partly associated with the temperature increase seen in Fig. 9a. This feature is likely due to aerosol induced changes in the Brewer–Dobson circulation in the low latitude UTLS. The region of warming in the stratosphere above the tropical tropopause can influence wave propagation and dissipation. There are also significant dynamical changes in the NH subtropics associated with the ASM that are likely modifying the synoptic-scale Rossby wave flux (see discussion below).

Fu et al. (2006) suggested that the Tibetan Plateau provides the main pathway for cross-tropopause transport. Deep convection occurs frequently over the Bay of Bengal and the Indian subcontinent during the ASM. Transport by monsoon convection produces high concentrations of H_2O and CO and relatively low O_3 concentrations in the upper troposphere. However, the highest water vapor concentrations in the lower stratosphere are observed to be located north of the monsoon region (over Tibetan Plateau). The proposed mechanism for this northward displacement is explained as water vapor (including other chemical constituents) transport by monsoon convection to the UT and then pseudo-isentropic transport northward to the extra tropical tropopause break north of the Tibetan Plateau. Park et al. (2009) used CO from observations and model simulations as a tracer to investigate the transport pathways during the ASM and suggested an alternative explanation. The observed enhancement of CO in the UTLS over the South Asian monsoon region originates from strong convective transport from

ACPD
12, 30081–30117, 2012

the boundary layer up to ∼200 hPa. The majority of this CO-rich air detrains in the upper troposphere. Some fraction of the air is advected by large scale upward motion on the eastern side of the anticyclone. The air that reaches 100 hPa is transported to the west and effectively gets confined within the anticyclonic circulation in the UTLS region. Park et al. (2007) also identified upwelling through the NH tropical tropopause during the ASM in ERA40 reanalyses and CAM3 simulations.

The results presented here broadly agree with the transport picture presented by Park et al. (2009), the primary route for tracers into the tropical tropopause layer (TTL) in the ASM region is via the convective zone on the southern flank of the Himalayas (15–30° N). A prominent feature seen in Fig. 9 is the increase in vertical transport over this region, which reaches the TTL and penetrates into the stratosphere. A large fraction of this circulation increase results from aerosol induced enhancement of the convection. However, the circulation increase above 200 hPa seen in Fig. 9 cannot be simply attributed to a change in the anticyclone. The zonal average over 60–120° E and 70–100° E (not shown) shows that the tropopause is elevated noticeably over the region of increased convective activity on the southern flank of the Himalayas. This indicates that convection is extending above 200 hPa in this region. The tropopause height increase can also be attributed in part to an intensification of the Brewer–Dobson circulation evident in Fig. 9, which exhibits increased poleward and downward transport in the subtropics which has to be balanced by more tropical upwelling (not necessarily at the equator). The increased Brewer–Dobson circulation implies an increase in wave drag. From the change in the zonal wind (not shown) it appears that both orographic gravity wave drag and synoptic scale Rossby wave drag have been modified due to aerosols. The former is due to an increase in the surface westerlies over India and the latter is due to an intensification of the subtropical jet and the associated change in vertical shear.

The meridional circulation anomaly between the equator and 30° N seen in Fig. 9 can be interpreted as the result of increased convective heating around 20–25° N. It drives a thermally direct circulation (like the Hadley circulation) and is subject to the same

ACPD
12, 30081–30117, 2012

asymmetry that is discussed by Lindzen and Hou (1988). Namely that it is centered off the equator so that there is a single dominant circulation cell on the equatorward side. The convective heating on the southern flanks of the Himalayas is a secondary tropical heating maximum, the primary one being in the ITCZ. The associated thermally direct circulation partly explains the extension of the circulation above 200 hPa since on longer timescales it satisfies an elliptic streamfunction equation, like the Hadley circulation, and exhibits non-locality with respect to the heating that forces it (Eliassen, 1951). The intensification of this secondary circulation contributes to the decreased ascent around 5° N, but it should be noted that the change in the Hadley circulation produced by aerosols is small and there is no significant change in its spatial structure.

Figure 9a also shows a cold stratospheric temperature anomaly above a warm tropospheric temperature anomaly around 30–40° N and 30–40° S. This structure is a manifestation of a "Gill-type solution" identified by Park et al. (2007) where two anticyclonic vortices on both sides of the equator are induced by a near equatorial heat source, from deep convection, lying to the east. Analysis of the CTRL – Ham-off geopotential and horizontal circulation difference at 100 hPa for June–September in our simulations (not shown) identifies two positive anomalies corresponding to a weaker anticyclone in the SH which mirrors a stronger anticyclone in the NH. Aerosols amplify the anticyclonic circulation in both hemispheres by intensifying deep convective heating in the regions of the ASM and north of Indonesia.

Warming of the tropical cold point tropopause seen in the present study agrees with a geo-engineering study by Heckendorn et al. (2009) which demonstrated that continuous emission of sulfur into the tropical lower stratosphere would lead to increased cold point temperatures. Warming of this sensitive region would then induce moistening of the stratosphere which is apparent in Fig. 9b.

To further diagnose the impact of aerosols on UTLS vapor we analyzed water vapour anomalies as obtained from difference between CTRL and HAM-off simulations at different pressure levels. Figure 10a–e shows water vapor anomalies at 155 hPa, 132 hPa, 110 hPa, 90 hPa and 70 hPa, respectively. There are positive water vapor anomalies

ACPD
12, 30081–30117, 2012

(0.2–3 ppmv) in the ASM anticyclone throughout the UTLS region induced by aerosols. Using the CAM3 climate model, Liu et al. (2009) demonstrated that increasing sulfate and soot pollution lead to increase in lower stratospheric water vapour ∼ 0.3 ppmv (10 %) and ∼ 0.6 ppmv (20 %), respectively. These results are in agreement with the present study. Above the tropopause there is a noticeable increase in water vapor between the equator and 15° N (Fig. 10d). This structure appears to be a horizontal transport feature the source of which is moisture injected into the lower tropical stratosphere over the South China Sea as well as Northern India and the Himalayas. Figure 10c shows that this feature is not transported from below. From Fig. 10a–e it is clear that aerosol enhances transport of water vapor into the lower stratosphere through the northern edge of the tropical tropopause inside the ASM anticyclone.

Figure 10f shows the distribution of aerosol induced changes in precipitation (averaged over the ASM). There are negative precipitation anomalies (−1 to −3 mm day^{-1}) to the South of India and extending northward along its eastern half. There is a small decrease over Northern India and the Tibetan Plateau west of 90° E (about −1 mm day^{-1}). This feature is most likely due to weakening of Hadley circulation as indicated in Fig. 9. The positive precipitation anomalies (0–3 mm day^{-1}) are over Western India which extends across it to the north-east around 20° N. At the eastern end of the anticyclone region (90–100° E and 12–30° N) there is significant increase in precipitation anomalies in the range of 4–5 mm day^{-1}. The positive vertical upwelling anomaly seen in Fig. 9 around 20° N is most intense between 90° E and 100° E and is associated with the increased convection indicated by this precipitation anomaly. The weakening of the Hadley circulation applies to both the primary branch and the weak northern branch. This helps to intensify the convective system in question since the upwelling increases. However, aerosols are modifying the convection as well so the increase in the secondary thermally direct circulation at the base of the Himalayas is not due just to changes in the Hadley circulation. As with the Hadley circulation there is a feedback from the non-local thermally direct circulation onto the convection, which acts to intensify it by through increased vertical upwelling. The region of increased precipitation also

ACPD
12, 30081–30117, 2012

extends over the South China Sea (1–3 mm day^{-1}). Simultaneous analysis of aerosol induced circulation changes (in Fig. 9a, b) and precipitation changes (in Fig. 10f) shows increased precipitation anomalies over the region of strong convection 15–30° N. Negative precipitation anomalies are observed in the region of reduced upwelling (5–10° N). However Lau et al. (2006) reported that rainfall response is not just a direct response to local aerosol forcing, but rather the result of a large scale dynamical adjustment to aerosol initiated horizontal and vertical heating gradients to the atmosphere and land surface, modulating the climatological seasonal heating in spring and summer. So the impact of aerosols during ASM on precipitation requires a more comprehensive analysis which is beyond the scope of this study.

4 Conclusions

An Eight member ensemble of ECHAM5-HAMMOZ simulations for the year 2003 is analyzed to study the transport of aerosols during Asian summer monsoon in the UTLS. Simulations show persistent maxima in black carbon, organic carbon, sulfate, and mineral dust aerosols within the anticyclone in the UTLS throughout summer. Model simulations indicate the transport of boundary layer aerosol pollutant by ASM convection to the UTLS. The evidence of ASM transport of aerosols in the stratosphere is observed in HALOE and SAGE II aerosol extinction. Model simulations and satellite data shows that high concentrations of BC, OC, SO_4^{2-} and mineral dust in the stratosphere extend to low latitudes and are transported across the equator poleward and downward in the Southern Hemisphere to ~30° S. Variations in all four types of aerosols in the anticyclone are closely related to deep convection.

Maxima in Ice Water Content (IWC) and Ice Crystal Number Concentration (ICNC) collocated with aerosol maximum indicate that transport of aerosol and water vapour rich air by deep convection may enhance high level cloud ice formation in the Northern Hemisphere subtropics. As cloud formation and its microphysical properties are strongly influenced by the availability of aerosols. Changes in cloud properties have

ACPD
12, 30081–30117, 2012

an impact on the hydrological cycle and climate. These aspects require more detailed analysis which is beyond the scope of this study.

The impact of aerosols in the UTLS region is analyzed by computing difference between simulations with aerosol loading (CTRL) and without aerosol loading (HAM-off). Transport of anthropogenic aerosols into the UTLS produces a complex response in temperature, water vapour and cloud ice in this region. There is warming of the tropical tropopause and the lower tropical stratosphere which is associated with direct and indirect effects of aerosols on transport and dynamics. A notable feature is the increased vertical transport between 15–30° N, which reaches into the tropical lower stratosphere. This is the primary transport pathway into the tropical lower stratosphere noted by Park et al. (2009) with the region of deep convection to the north of Indonesia acting as another pathway. In addition to convection, the transport change in this region involves diabatic circulation changes in the troposphere and the stratospheric Brewer–Dobson circulation near the tropopause. The effect of aerosols in the ASM region is to reduce vertical upwelling around 5° N. This reduces transport of water vapour into the mid troposphere near the equator. At the same time there is increased transport of water vapour around 15–30° N.

Recently it became clear that cirrus clouds significantly affect the global energy balance and climate, due to their influence on the atmospheric thermal structure. Hence, anthropogenic aerosols transported by ASM convection to the UTLS region may impact the hydrological cycle and climate. Several studies (e.g. Randall et al., 1989; Ramaswamy and Ramanathan, 1989; Liu et al., 2003a,b) point out that cirrus clouds are likely to have great impact on the radiation and hence the intensity of the large-scale circulation in the tropics. In particular, some studies (Su et al., 2011) suggest that pollution acts to warm the TTL and could lead to a moistening of the stratosphere. In agreement with these studies our simulations shows increase in tropical tropopause temperature by 0.3–2.5 K and an associated increase water vapor 0.2–3 ppmv.

Aerosols induce a weakening of the Hadley circulation, as noted in previous studies (e.g. Ramanathan et al., 2005; Bollasina et al., 2011), and an intensification of

ACPD
12, 30081–30117, 2012

a secondary thermally direct circulation associated with the region of strong convection on the southern flanks of the Himalayas (15–30° N). Significant positive precipitation anomalies (5–7 mm day^{-1}) are observed over this region of intensified convection, at the eastern end of the anticyclone (90–100° E). There are negative precipitation anomalies (−1 to −3 mm day^{-1}) to the South of India and extending northward along its eastern half. There is a small decrease over Northern India and the Tibetan Plateau west of 90° E (about −1 mm day^{-1}). Negative precipitation anomalies are collocated with reduced upwelling around 5–10° N. This is most likely due to weakening of Hadley circulation upwelling at these latitudes. The impact of aerosols on precipitation requires a more detailed study to be done later.

Acknowledgements. S. Fadnavis acknowledge with gratitude B. N. Goswami, Director IITM for his encouragement during the course of this study. Authors thank SAGE II and HALOE team for providing data.

References

Andrews, D. G., Holton, J. R., and Leovy, C. B.: Middle Atmosphere Dynamics, Academic Press, New York, 489 pp., 1987.

Antuña, J. C., Robock, A., Stenchikov, G. L., Thomason, L. W., and Barnes, J. E.: Lidar validation of SAGE II aerosol measurements after the 1991 Mount Pinatubo eruption, J. Geophys. Res., 107, 4194, doi:10.1029/2001JD001441, 2002.

Auvray, M., Bey, I., Llull, E., Schultz, M. G., and Rast, S.: A model investigation of tropospheric ozone chemical tendencies in long-range transported pollution plumes, J. Geophys. Res., 112, D05304, doi:10.1029/2006JD007137, 2007.

Bollasina, M. A., Ming, Y., and Ramaswamy, V.: Anthropogenic Aerosols and the weakening of the South Asian summer monsoon, Science, 334, 502–505, doi:10.1126/science.1204994, 2011.

Bowman, K. P.: Transport of carbon monoxide from the tropics to the extratropics, J. Geophys. Res., 111, D02107, doi:10.1029/2005JD006137, 2006.

Dentener, F., Kinne, S., Bond, T., Boucher, O., Cofala, J., Generoso, S., Ginoux, P., Gong, S., Hoelzemann, J. J., Ito, A., Marelli, L., Penner, J. E., Putaud, J.-P., Textor, C., Schulz, M.,

ACPD
12, 30081–30117, 2012

van der Werf, G. R., and Wilson, J.: Emissions of primary aerosol and precursor gases in the years 2000 and 1750 prescribed data-sets for AeroCom, Atmos. Chem. Phys., 6, 4321–4344, doi:10.5194/acp-6-4321-2006, 2006.

Dodion, J., Fussen, D., Vanhellemont, F., Bingen, C., Mateshvili, N., Gilbert, K., Skelton, R., Turnball, D., McLeod, S. D., Boone, C. D., Walker, K. A., and Bernath P. F.: Aerosols and clouds in the upper troposphere-lower stratosphere region detected by GOMOS and ACE: intercomparison and analysis of the years 2004 and 2005, Adv. Space Res., 42, 1730–1742, doi:10.1016/j.asr.2007.09.027, 2008.

Eliassen, A.: Slow thermally and frictionally controlled circulation in a circular vortex, Astrophys. Norv., 5, 19–60, 1951.

Fu, R., Hu, Y., Wright, J. S., Jiang, J. H., Dickinson, R. E., Chen, M., Filipiak, M., Read, W. G., Waters, J. W., and Wu, D. L.: Short circuit of water vapor and polluted air to the global stratosphere by convective transport over the Tibetan Plateau, P. Natl. Acad. Sci. USA, 103, 5664–5669, doi:10.1073/pnas.0601584103, 2006.

Gettelman, A., Kinnison, D. E., Dunkerton, T. J., and Brasseur, G. P.: The impact of monsoon circulations on the upper troposphere and lower stratosphere, J. Geophys. Res., 109, D22101, doi:10.1029/2004JD004878, 2004.

Haynes, P. and Shuckburgh, E.: Effective diffusivity as a diagnostic of atmospheric transport, Part II: Troposphere and lower stratosphere, J. Geophys. Res., 105, 22795–22810, doi:10.1029/2000JD900092, 2000.

Heckendorn, P., Weisenstein, D., Fueglistaler, S., Luo, B. P., Rozanov, E., Schraner, M., Thomason, L. W., and Peter, T.: The impact of geoengineering aerosols on stratospheric temperature and ozone, Environ. Res. Lett., 4, 045108, doi:10.1088/1748-9326/4/4/045108, 2009.

Hervig, M. E., Russell III, J. M., Gordley, L. L., Daniels, J., Drayson, S. R., and Park, J. H.: Aerosol effects and corrections in the Halogen Occultation Experiment, J. Geophys. Res., 100, 1067–1079, 1995.

Horowitz, L. W., Walters, S., Mauzerall, D. L., Emmons, L. K., Rasch, P. J., Granier, C., Tie, X., Lamarque, J., Schultz, M. G., Tyndall, G. S., Orlando, J. J., and Brasseur, G. P.: A global simulation of tropospheric ozone and related tracers: description and evaluation of MOZART, version 2, J. Geophys. Res., 108, 4784, doi:10.1029/2002JD002853, 2003.

IPCC (Intergovernmental Panel on Climate Change): Climate Change 2007 – The Physical Science Basis, Contribution of Working Group 1 to the Fourth Assessment Report of the

ACPD
12, 30081–30117, 2012

Intergovernmental Panel on Climate Change, Cambridge University Press, Cambridge, UK and New York, 2007.
Jeong, J. I., Park, R. J., Woo, J. H., Han, Y. J., and Yi, S. M.: Source contributions to carbonaceous aerosols in Korea, Atmos. Environ., 45, 1116–1125. 2011.
Kent, G. S., Trepte, C. R., Skeens, K. M., and Winker, D. M.: LITE and SAGE II measurements of aerosols in the Southern Hemisphere upper troposphere, J. Geophys. Res., 103, 19111–19127, doi:10.1029/98JD00364, 1998.
Kinnison, D. E., Brasseur, G. P., Walters, S., Garcia, R. R., Marsh, D. R., Sassi, F., Harvey, V. L., Randall, C. E., Emmons, L., Lamarque, J. F., Hess, P., Orlando, J. J., Tie, X. X., Randel, W., Pan, L. L., Gettelman, A., Granier, C., Diehl, T., Niemeier, U., and Simmons, A. J.: Sensitivity of chemical tracers to meteorological parameters in the MOZART-3 chemical transport model, J. Geophys. Res., 112, D20302, doi:10.1029/2006JD007879, 2007.
Kravitz, B., Robock, A., Shindell, D. T., and Miller, M. A.: Sensitivity of stratospheric geoengineering with black carbon to aerosol size and altitude of injection. J. Geophys. Res., 117, D09203, doi:10.1029/2011JD017341, 2012.
Kunze, M., Braesicke, P., Langematz, U., Stiller, G., Bekki, S., Brühl, C., Chipperfield, M., Dameris, M., Garcia, R., and Giorgetta, M.: Influences of the Indian summer monsoon on water vapor and ozone concentrations in the UTLS as simulated by chemistry-climate models, J. Climate, 23, 3525–3544, 2010.
Lau, K. M. and Kim, K. M.: Observational relationships between aerosol and Asian Monsoon rainfall, and circulation, Geophys. Res. Lett., 33, L21810, doi:10.1029/2006GL027546, 2006.
Lau, K. M., Kim, M. K., and Kim, K. M.: Asian summer monsoon anomalies induced by aerosol direct forcing: the role of the Tibetan Plateau, Clim. Dynam., 26, 855–864, 2006.
Li, Q., Jiang, J. H., Wu, D. L., Read, W. G., Livesey, N. J., Waters, J. W., Zhang, Y., Wang, B., Filipiak, M. J., Davis, C. P., Turquety, S., Wu, S., Park R. J., Yantosca R. M., and Jacob D. J.: Convective outflow of South Asian pollution: a global CTM simulation compared with EOS MLS observations, Geophys. Res. Lett., 32, L14826, doi:10.1029/2005GL022762, 2005.
Lin, H. and Leaitch, R.: Development of an in-cloud aerosol activation parameterization for climate modelling, in: Proc. WMO Workshop on Measurements of Cloud Properties for Forecasts of Weather, Air Quality and Climate, Mexico City, 13562–13563, 23–27 June 1997.
Lindzen, R. S. and Hou, A. Y.: Hadley circulations for zonally averaged heating centered off the equator, J. Atmos. Sci., 45, 2416–2427, 1988.

ACPD
12, 30081–30117, 2012

Liu, H. L., Wang, P. K., and Schlesinger, R. E.: A numerical study of cirrus clouds, Part I: Model description, J. Atmos. Sci., 60,1075–1084, 2003a.
Liu, H. L., Wang, P. K., and Schlesinger, R. E.: A numerical studyof cirrus clouds, Part II: Effects of ambient temperature, stability, radiation, ice microphysics, and microdynamics on cirrus evolution, J. Atmos. Sci., 60, 1097–1119, 2003b.
Liu, J. and Diamond, J.: China's environment in a globalizing world, Nature, 435, 1179–1186, 2005.
Liu, X., Penner, J. E., and Wang M.: Influence of anthropogenic sulfate and black carbon on upper tropospheric clouds in the NCAR CAM3 model coupled to the IMPACT global aerosol model, J. Geophys. Res., 114, D03204, doi:10.1029/2008JD010492, 2009.
Logan, J.: An analysis of ozonesonde data for the troposphere: recommendations for testing 3-D models and development of a gridded climatology for tropospheric ozone, J. Geophys. Res., 104, 16115–16149, 1999.
Lohmann, U. and Roeckner, E.: Design and performance of a new cloud microphysics scheme developed for the ECHAM general circulation model, Clim. Dynam., 12, 557–572, 1996.
Lohmann, U., Feichter, J., Chuang, C. C., and Penner, J. E.: Prediction of the number of cloud droplets in the ECHAM GCM, J. Geophys. Res., 104, 9169–9198, doi:10.1029/1999JD900046, 1999.
Menon, S., Hansen, J., Nazarenko, L., and Luo, Y.: Climate effects of black carbon aerosols in China and India, Science, 297, 2250–2253, 2002.
Minschwaner, K., Dessler, A. E., Elkins, J. W., Volk, C. M., Fahey, D. W., Loewenstein, M., Podolske, J. R., Roche, A. E., and Chan, K. R.: Bulk properties of isentropic mixing into the tropics in the lower stratosphere, J. Geophys. Res., 101, 9433–9439, doi:10.1029/96JD00335, 1996.
O'Sullivan, D. and Dunkerton, T. J.: The influence of the quasi-biennial oscillation on global constituent distributions, J. Geophys. Res., 102, 21731–21743, doi:10.1029/97JD01689, 1997.
Oberbeck, V. R., Livingston, J. M., Russell, P. B., Pueschel, R. F., Rosen, J. N., Osborn, M. T., Kritz, M. A., Snetsinger, K. G., and Ferry, G. V.: SAGE II aerosol validation: selected altitude measurements, including particle micromeasurements, J. Geophys. Res., 94, 8367–8380, doi:10.1029/JD094iD06p08367, 1989.
Park, M., Randel, W. J., Kinnison, D. E., Garcia, R. R., and Choi, W.: Seasonal variation of methane, water vapor, and nitrogen oxides near the tropopause: satellite observations and model simulations, J. Geophys. Res., 109, D03302, doi:10.1029/2003JD003706, 2004.

ACPD
12, 30081–30117, 2012

Park, M., Randel, W. J., Getteleman, A., Massie, S. T., and Jiang, J. H.: Transport above the Asian summer monsoon anticyclone inferred from aura microwave limb sounder tracers, J. Geophys. Res., 112, D16309, doi:10.1029/2006JD008294, 2007.

Park, M., Randel, W. J., Emmons, L. K., and Livesey, N. J.: Transport pathways of carbon monoxide in the Asian summer monsoon diagnosed from Model of Ozone and Related Tracers (MOZART), J. Geophys. Res., 114, D08303, doi:10.1029/2008JD010621, 2009.

Park, R. J., Kim, M. J., Jeong, J. I., Youn, D., and Kim, S.: A contribution of brown carbon aerosol to the aerosol light absorption and its radiative forcing in East Asia, Atmos. Eviron., 44, 1414–1421, 2010.

Pozzoli, L., Bey, I., Rast, J. S., Schultz, M. G., Stier, P., and Feichter, J.: Trace gas and aerosol interactions in the fully coupled model of aerosol-chemistry-climate ECHAM5- HAMMOZ: 1. Model description and insights from the spring 2001 TRACE-P experiment, J. Geophys. Res., 113, D07308, doi:10.1029/2007JD009007, 2008a.

Pozzoli, L., Bey, I., Rast, J. S., Schultz, M. G., Stier, P., and Feichter, J.: Trace gas and aerosol interactions in the fully coupled model of aerosol-chemistry-climate ECHAM5- HAMMOZ: 2. Impact of heterogeneous chemistry on the global aerosol distributions, J. Geophys. Res., 113, D07309, doi:10.1029/2007JD009008, 2008b.

Pozzoli, L., Janssens-Maenhout, G., Diehl, T., Bey, I., Schultz, M. G., Feichter, J., Vignati, E., and Dentener, F.: Re-analysis of tropospheric sulfate aerosol and ozone for the period 1980–2005 using the aerosol-chemistry-climate model ECHAM5-HAMMOZ, Atmos. Chem. Phys., 11, 9563–9594, doi:10.5194/acp-11-9563-2011, 2011.

Ramaswamy, V. and Ramanathan V.: Solar absorption of cirrus clouds and the maintenance of the tropical upper troposphere thermal structure, J. Atmos. Sci., 46, 2293–2310, 1989.

Ramanathan, V., Chung, C., Kim, D., Bettge, T., Buja, L., Kiehl, J. T., Washington, W. M., Fu, Q., Sikka, D. R., and Wild M.: Atmospheric brown clouds: impacts on South Asian climate and hydrological cycle, PNAS, 102, 5326–5333, doi:10.1073/pnas.0500656102, 2005.

Randall, D. A., Harshovardan, D. A., Dazlich, D. A., and Corsetti, T. G.: Interactions among radiation, convection, and large-scale dynamics in a general circulation model, J. Atmos. Sci., 46, 1943–1970, 1989.

Randel, W. J. and Park, M.: Deep convective influence on the Asian summer monsoon anticyclone and associated tracer variability observed with Atmospheric Infrared Sounder (AIRS), J. Geophys. Res., 111, D12314, doi:10.1029/2005JD006490, 2006.

ACPD
12, 30081–30117, 2012

Randel, W., Wu, F., Russell, J., Roche, A., and Waters J.: Seasonal cycles and QBO variations in stratospheric CH_4 and H_2O observed in UARS HALOE data, J. Atmos. Sci., 55, 163–185, 1998.

Randel, W. J., Park, M., Emmons, L., Kinnison, D., Bernath, P., Walker, K. A., Boone, C., and Pumphrey H.: Asian monsoon transport of pollution to the stratosphere, Science, 328, 611–613, 5978, doi:10.1126/science.1182274, 2010.

Rast, J., Schultz, M., Aghedo, A., Bey, I., Brasseur, G., Diehl, T., Esch, M., Ganzeveld, L., Kirchner, I., Kornblueh, L., Rhodin, A., Roeckner, E., Schmidt, H., Schroede, S., Schulzweida, U., Stier, P., and van Noije, T.: Evaluation of the tropospheric chemistry general circulation model ECHAM5–MOZ and its application to the analysis of the inter-annual variability in tropospheric ozone from 1960–2000 chemical composition of the troposphere for the period 1960–2000 (RETRO), MPI-Report (Reports on Earth System Science), in preparation, 2012.

Roeckner, E., Bauml, G., Bonaventura, L., Brokopf, R., Esch, M., Giorgetta, M., Hagemann, S., Kirchner, I., Kornblueh, L., Manzini, E., Rhodin, A., Schlese, U., Schulzweida, U., and Tompkins, A.: The atmospehric general circulation model ECHAM5: Part 1, Tech. Rep. 349, Max Planck Institute for Meteorology, Hamburg, 2003.

Rosenfield, J. E., Considine, D. B., Schoeberl, M., and Browell, E.: The impact of subvisible cirrus clouds near the tropical tropopause on stratospheric water vapor, Geophys. Res. Lett., 25, 1883, doi:10.1029/98GL01294, 1998.

Russell, J. M., Gordley, L. L., Park, J. H., Drayson, S. R., Hesketh, W. D. Cicerone, R. J., Tuck, A. F., Frederick, J. E., Harries, J. E., Crutzen P. J.: The Halogen occultation Experiment, J. Geophys. Res., 98, 10777–10797, 1993.

Schultz, M., Heil, A., Hoelzemann, J., Spessa, A., Thonicke, K., Goldammer, J., Held, A., Pereira, J., and van het Bolscher, M.: Global wildland fire emissions from 1960 to 2000, Global Biogeochem. Cyc., 22, 1–17, doi:10.1029/2007GB003031, 2008.

Stier, P., Feichter, J., Kinne, S., Kloster, S., Vignati, E., Wilson, J., Ganzeveld, L., Tegen, I., Werner, M., Balkanski, Y., Schulz, M., Boucher, O., Minikin, A., and Petzold, A.: The aerosol-climate model ECHAM5-HAM, Atmos. Chem. Phys., 5, 1125–1156, doi:10.5194/acp-5-1125-2005, 2005.

Su, H., Jiang, J. H., Liu, X., Penner, J. E., Read, W. G., Massie, S., Schoeberl, M. R., Colarco, P., Livesey, N. J., and Santee, M. L.: Observed increase of TTL temperature and water vapor in polluted clouds over Asia, J. Climate, 24, 2728–2736, doi:10.1175/2010JCLI3749.1, 2011.

ACPD
12, 30081–30117, 2012

Terao, Y. and Logan, J. A.: Consistency of time series and trends of stratospheric ozone as seen by ozonesonde, SAGE II, HALOE, and SBUV(/2), J. Geophys. Res., 112, D06310, doi:10.1029/2006JD007667, 2007.

Venkataraman, C., Habib, G., Eiguren-Fernandez, A., Miguel, A. H., and Friedlander, S. K.: Residential biofuels in South Asia: carbonaceous aerosol emissions and climate impacts, Science, 307, 1454, doi:10.1126/science.1104359, 2005.

Vernier, J. P., Thomason, L. W., and Kar, J.: CALIPSO detection of an Asian tropopause aerosol layer, Geophys. Res. Lett., 38, L07804, doi:10.1029/2010GL046614, 2011.

Vignati, E., Wilson, J., and Stier, P.: M7: an efficient size-resolved aerosol microphysics module for large-scale aerosol transport models, J. Geophys. Res., 109, D22202, doi:10.1029/2003JD004485, 2004.

WMO (World Meteorological Organization): International Meteorological Vocabulary, 2nd edn., Geneva, Switzerland, 784pp., 1992.

Xiong, X., Houweling, S., Wei, J., Maddy, E., Sun, F., and Barnet, C.: Methane plume over south Asia during the monsoon season: satellite observation and model simulation, Atmos. Chem. Phys., 9, 783–794, doi:10.5194/acp-9-783-2009, 2009.

Yin, Y., Carslaw, K. S., and Feingold, G.: Vertical transport and processing of aerosols in a mixed-phase convective cloud and the feedback on cloud development, Q. J. Roy. Meteor. Soc., 131, 221–246, 2005.

ACPD
12, 30081–30117, 2012

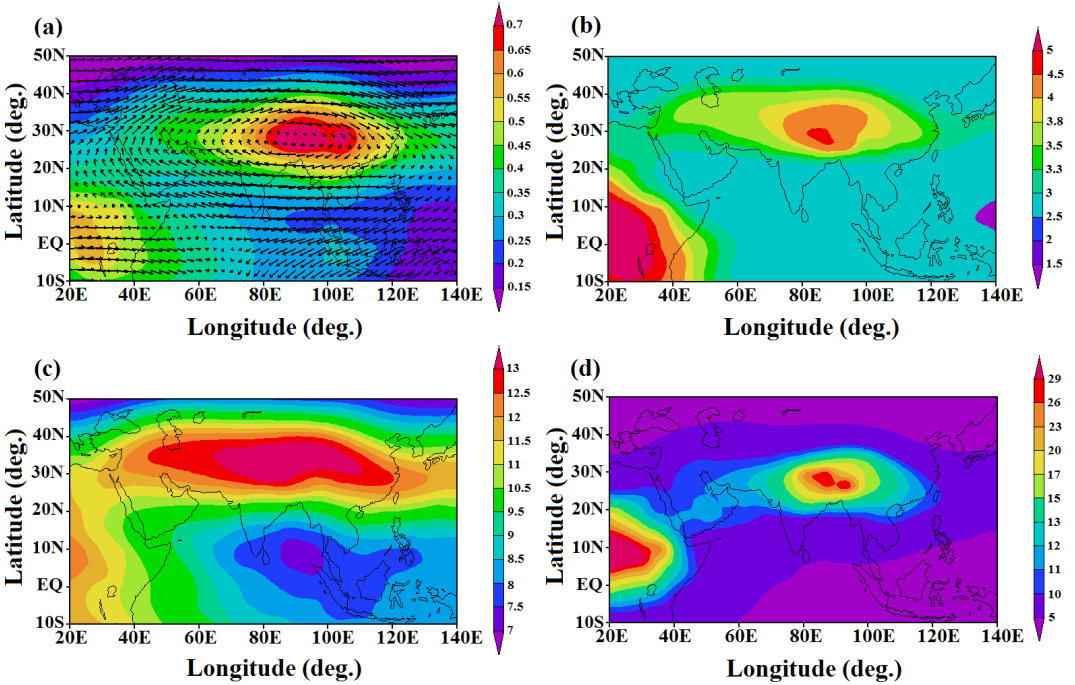

Fig. 1. Horizontal structure of June–September 2003 averages at 110 hPa of aerosol concentrations (ng m^{-3}): **(a)** BC and horizontal wind fields (shown as vectors), **(b)** OC, **(c)** SO_4^{2-} and **(d)** mineral dust.

ACPD
12, 30081–30117, 2012

Transport of aerosol pollution in the UTLS

S. Fadnavis et al.

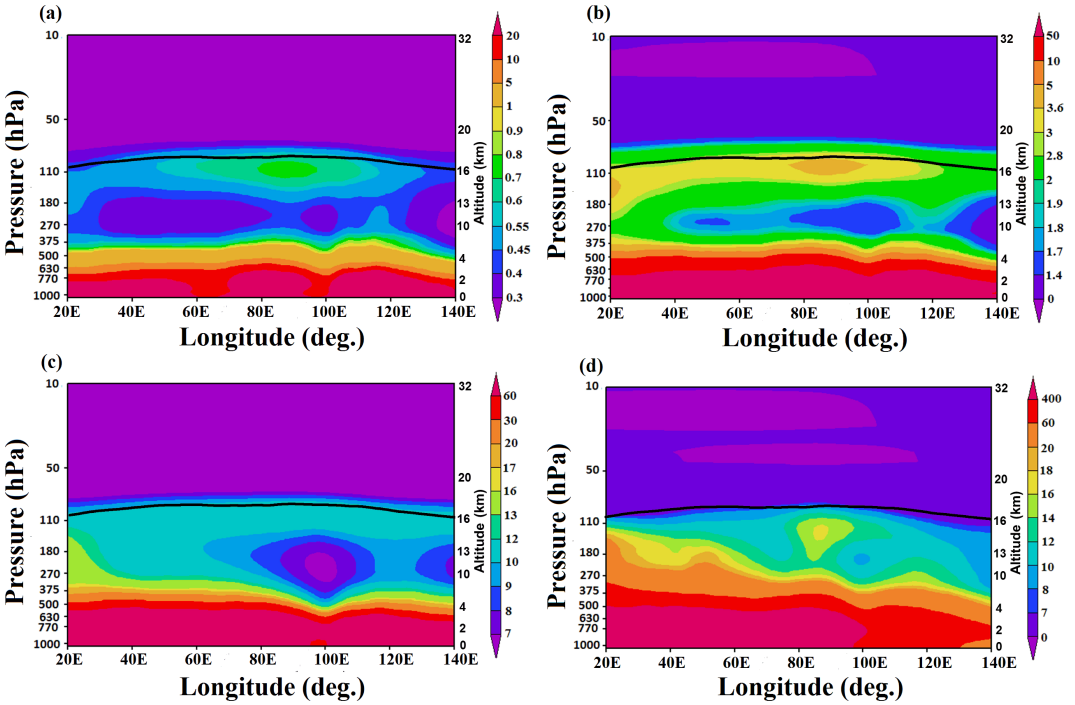

Fig. 2. Longitude-pressure section (averaged for June–September and 15–35° N) of concentrations (ng m^{-3}) of **(a)** BC aerosols, **(b)** OC aerosols, **(c)** SO_4^{2-} and **(d)** mineral dust aerosols. The black line marks the latitudinally averaged tropopause showing increased height in the ASM region.

ACPD
12, 30081–30117, 2012

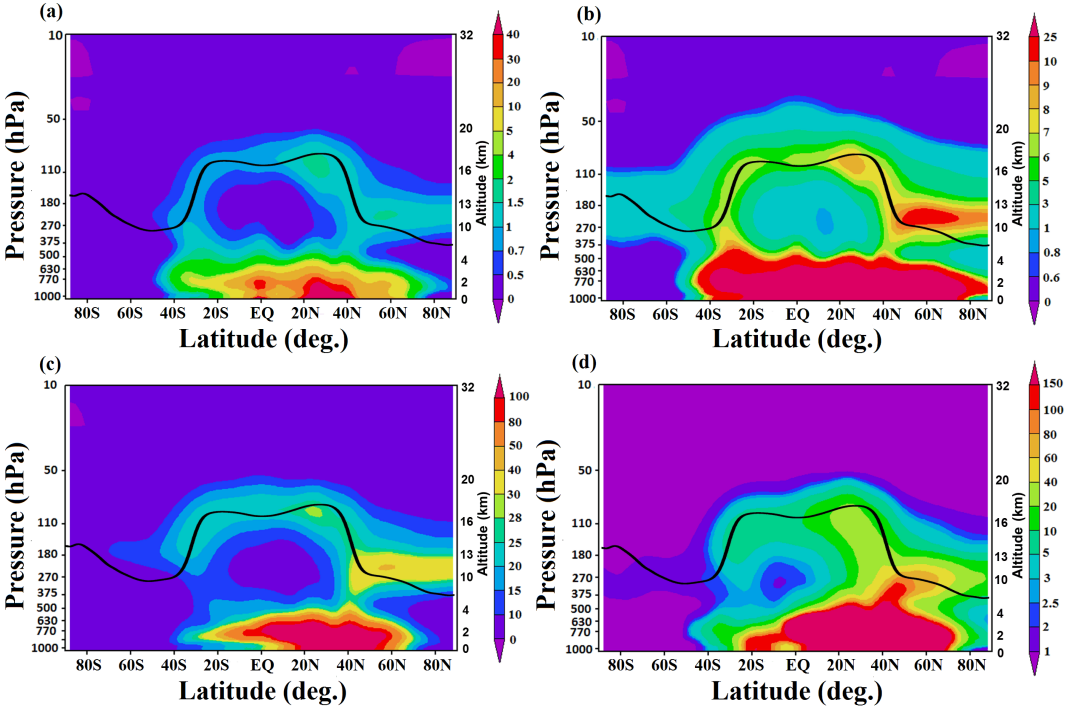

Fig. 3. Latitude-pressure section (averaged for June–September and 60–120° E) of concentrations ($\mu g\,m^{-3}$) of **(a)** BC aerosols **(b)** OC aerosols **(c)** SO_4^{2-} **(d)** mineral dust aerosols. The black line marks the longitudinally averaged tropopause showing increased height in the ASM region.

ACPD
12, 30081–30117, 2012

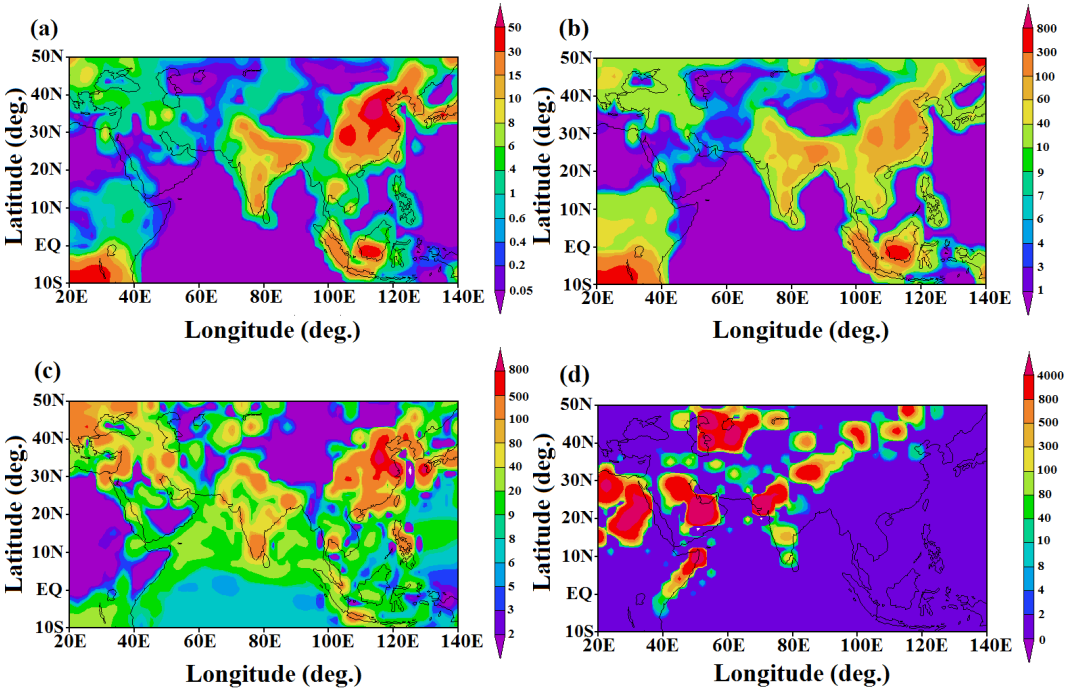

Fig. 4. Distribution of emission mass flux (mg month^{-1}) averaged for June–September 2003 for **(a)** BC, **(b)** OC, **(c)** SO_4^{2-}, and **(d)** mineral dust.

ACPD
12, 30081–30117, 2012

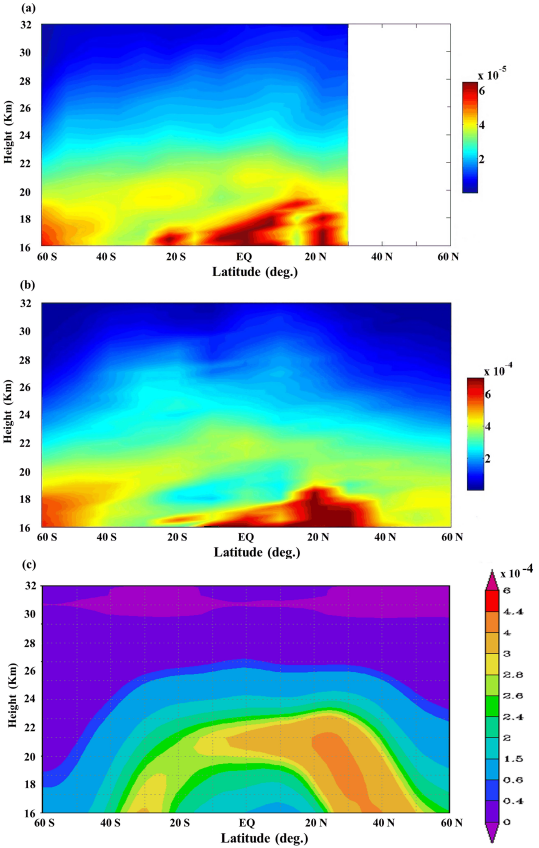

Fig. 5. Latitude-pressure section (averaged for June–September and 60–120° E) of aerosol extinction (km^{-1}) as obtained from **(a)** HALOE 5.26 µm for the year 2003 **(b)** SAGE II 0.525 µm **(c)** ECHAM5-HAMMOZ simulations 0.550 µm for the year 2003 at the altitude 16–32 km.

ACPD
12, 30081–30117, 2012

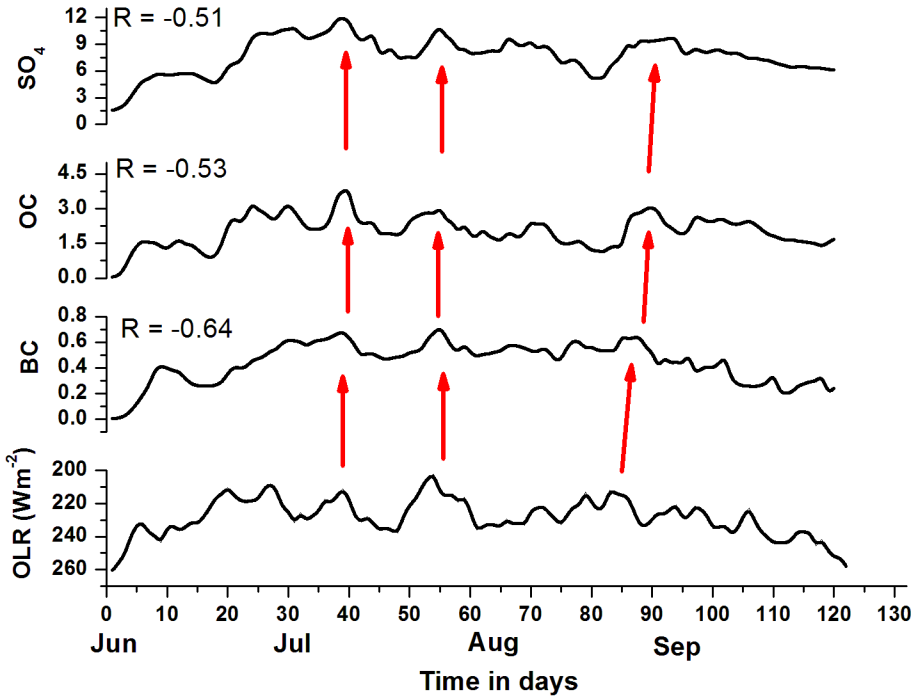

Fig. 6. Time series of OLR averaged over (15–30° N, 60–120° E) and ECHAM5-HAMMOZ simulated concentrations (ng m^{-3}) of BC, OC, SO_4^{2-}, averaged over 20–30° N and 60–120° E. Note that the scale for OLR is inverted. The anti-correlation coefficient of BC, OC, SO_4^{2-}, with OLR is indicated at the top of the each panel.

ACPD
12, 30081–30117, 2012

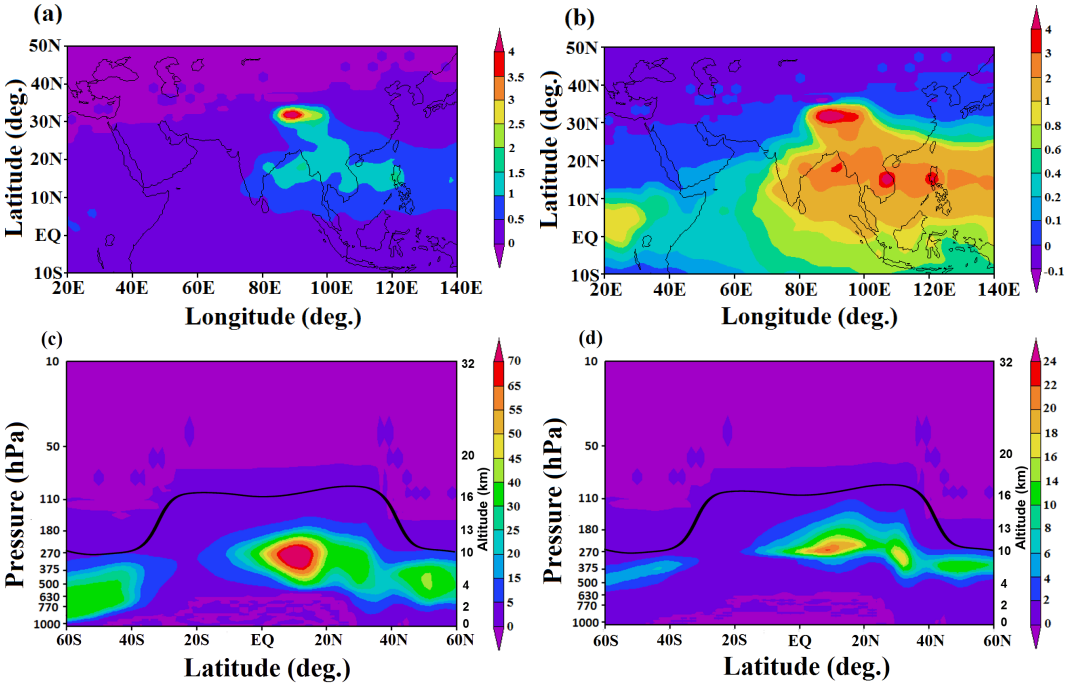

Fig. 7. (a) Horizontal structure as obtained from ECHAM5-HAMMOZ CTRL simulations (averaged for ASM) of **(a)** ice water content (mg m^{-3}) at 110 hPa **(b)** ice crystal number concentration (1 mg^{-1}) at 110 hPa **(c)** latitude-pressure cross section (averaged for June–September and 60–120° E) of ice water content (mg m^{-3}) **(d)** latitude–pressure cross section (averaged for June–September and 60–120° E) of ice crystal number concentration (ICNC) (1 mg^{-1}).

ACPD
12, 30081–30117, 2012

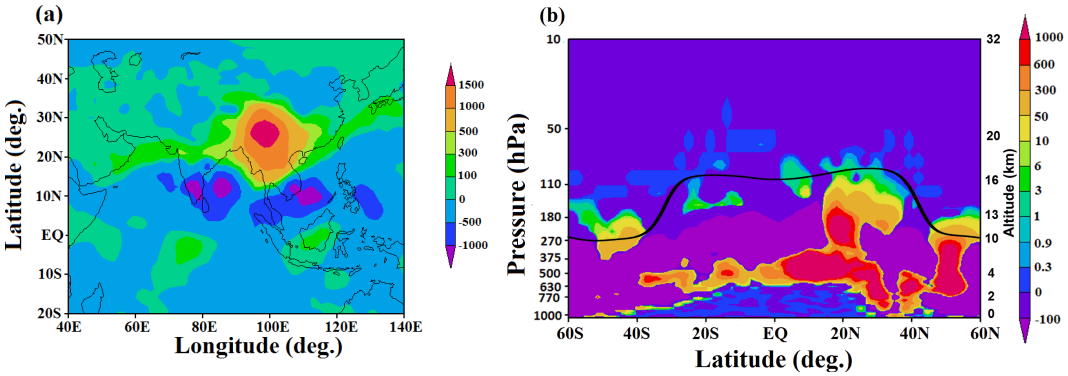

Fig. 8. Spatial structure of mean cloud ice ($\mu g m^{-3}$) anomalies as obtained from ECHAM5-HAMMOZ CTRL – HAM-off runs during ASM. **(a)** Pressure level slice at 181 hPa. **(b)** latitude-pressure distribution averaged over 60–120° E.

ACPD
12, 30081–30117, 2012

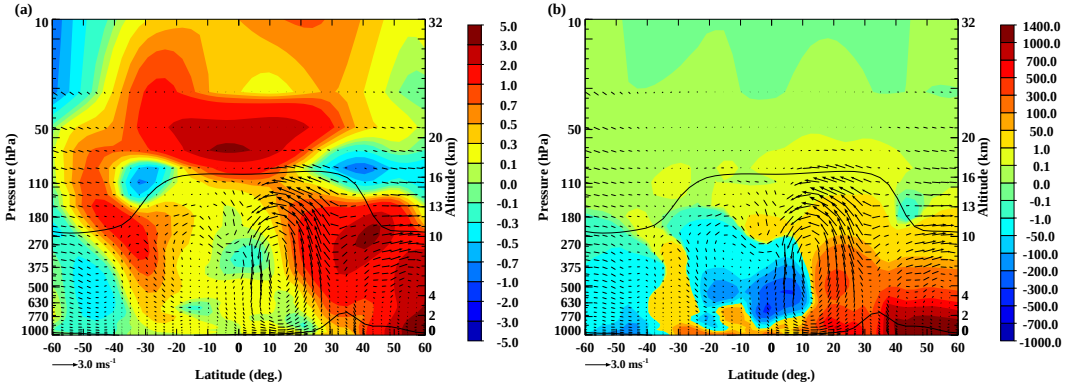

Fig. 9. Latitude-pressure structure (averaged over 60–120° E) of difference between ECHAM5-HAMMOZ CTRL – HAM-off runs during ASM for **(a)** temperature (K) and **(b)** water vapour (ppmv). The meridional circulation is shown as a vector field. (The vertical velocity field has been scaled by 300 and the units are $m s^{-1}$.)

ACPD
12, 30081–30117, 2012

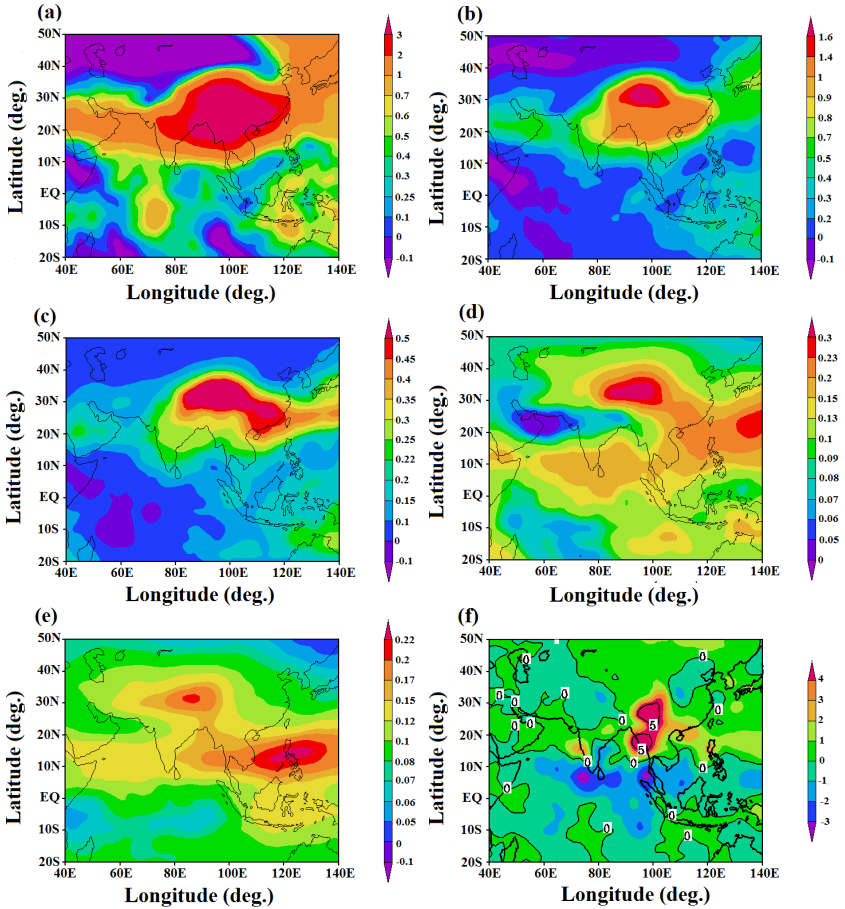

Fig. 10. (a) Spatial structure of mean water vapor (ppmv) anomalies obtained from ECHAM5-HAMMOZ CTRL – HAM-off runs during ASM at **(a)** 155 hPa, **(b)** 132 hPa, **(c)** 110 hPa, **(d)** 90 hPa, **(e)** 70 hPa and **(f)** spatial distribution of mean (JJAS) precipitation (mm/day) anomalies.

ACPD
12, 30081–30117, 2012